The 2015 World Congress on
Advances in Structural Engineering and Mechanics (ASEM15)
Incheon, Korea, August 25-29, 2015

A New Methodology in Seismic Torsion Design of Building Structures

*Han Seon Lee[1)] and Kyung Ran Hwang[2)]

[1), 2)] *School of Civil, Environmental, and Architectural Engineering, Korea University, Seoul, 136-713, Korea*
[1)] *hslee@korea.ac.kr*

ABSTRACT

An experimental research using a 1:5 scale five-story reinforced concrete building model with the irregularities of a soft/weak story and torsion at the ground story revealed that the design eccentricity given in the general codes can not represent the critical torsional behaviors not only because the range of eccentricities at the peak responses in the time histories of drift and base shear exceeded the range of eccentricity predicted by the code, but also because under severe ground excitations even very small eccentricity does not necessary translate into a small but significantly large drift at the edge frame. To overcome this problem, instead of using the eccentricity as design parameter, a completely new methodology in the design or control of torsionally unbalanced building structures is proposed by defining the design torsional moment in a direct relationship with the shear force given as an ellipse with the maximum points in its principal axes located by the two adjacent torsion-dominant modal spectral values. This approach provides a simple, transparent, and comprehensive design tool by enabling comparison between demand and supply.

1. INTRODUCTION

The severe damage and collapse of building structures in earthquake can occur through several phenomena, one of which is the torsion due to the eccentricity between the inertia force and resisting force. To prevent excessive deformation, damage, and collapse caused by torsion, the current seismic design code specifies two torsion design approaches: First, using equivalent lateral force (static) procedure, the structure is designed by the most adverse combination of the seismic forces for Eq. (1) and the design eccentricities for Eq. (2) as shown in Fig. 1(a). Second, using the dynamic analysis such as modal response spectrum analysis or time history analysis, the center of the mass (CM) at each story is assumed to be the positions, CM1~CM4 in Fig. 1(b). The most adverse results in deformations and member forces of the structure obtained from the dynamic analysis are used for design.

[1)] Professor
[2)] Graduate Student

$$V_D = C_S W \tag{1}$$

$$e_d = \alpha e_s + \beta b \quad \text{or} \quad e_d = \delta e_s - \beta b \tag{2}$$

where, V_D is the seismic base shear; C_S is the seismic coefficient; W is the effective seismic weight; e_d is the design eccentricity composed of static and accidental eccentricities; e_s is the static eccentricity determined as the distance between the CM and CS (center of stiffness); βb (=e_a) is the accidental eccentricity, which is included to consider torsional effects due to the uncertainty of CM and CS, the rotational component of ground motion, and other uncertainties not explicitly considered; b is the plan dimension of the building perpendicular to the direction of ground motion; and α, β, and δ are code-specified coefficients.

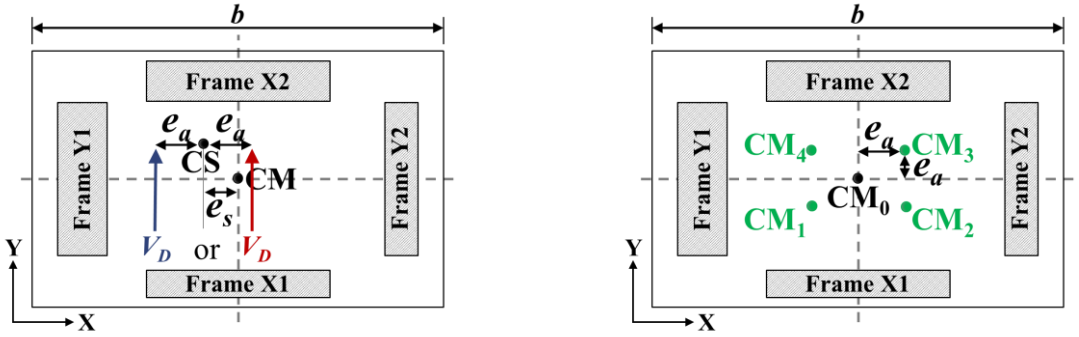

(a) Equivalent lateral force (static)analysis (b) Dynamic analysis

Fig. 1 Conventional torsion design approaches

Though the design eccentricity in Eq. (2) is based on the linear elastic behavior of the structure, the main concern is the control of the deformation and damage in the inelastic range. That is, the objective of torsion design is that the maximum drift or ductility demands in any part of the element of the torsionally unbalanced building do not exceed those of the torsionally balanced, under any circumstances. However, almost all researchers aimed at the reasonable determination of coefficient values, α, β, and δ in Eq. (2), to achieve such an objective, based on the assumption that the satisfaction of design requirements for load combinations of the seismic design story or base shear forces, V_D, and the torsional moment resulting from the design eccentricity ensures the desirable inelastic behavior under the severe earthquake.

The first study of this problem appeared in 1938 and continued in the late 50ties, with about 6 papers published from 1958 till 1970. Subsequently the number of pertinent publications started growing fast. Currently, the total number of publications on this subject in refereed international Journals and in major Conferences probably exceeds 700 as shown in Fig. 2. This large number must be attributed to the importance of torsion that adversely affects the vast majority of buildings with any type of eccentricity, to the new technologies applied for controlling torsional response and also to the many parameters affecting this problem (Anagnostopoulos el al. 2013). Areas of concern where the use of differing definitions or the making of diverging assumptions has resulted in a basic lack of agreement between the results and conclusions of the research (Rutenburg 1992 and Chandler et al. 1996).

Although it is difficult to find a sound rationale that the satisfaction of design requirements for four load combinations determined by Eq. (2) guarantees the desirable inelastic behavior, researchers and engineers have maintained the faith in efficacy of the design eccentricity for over 6 decades since the emergence of earthquake engineering as a new field of engineering.

In this study, to overcome the serious limitation of the conventional torsion design approach using the design eccentricity, a new simple, transparent, and comprehensive torsion design approach is proposed based on actual torsional behaviors obtained the shake-table test of a low-rise RC building model, which as a high degree of irregularity of soft story, weak story, and torsion at the ground story (Lee et al. 2011, 2013, and 2015).

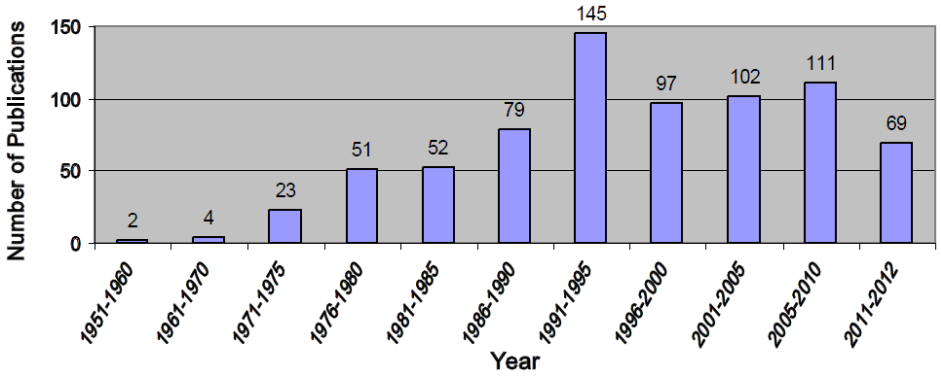

Fig. 2 Histogram of time distribution of publications on building torsion (Anagnostopoulos el al. 2013)

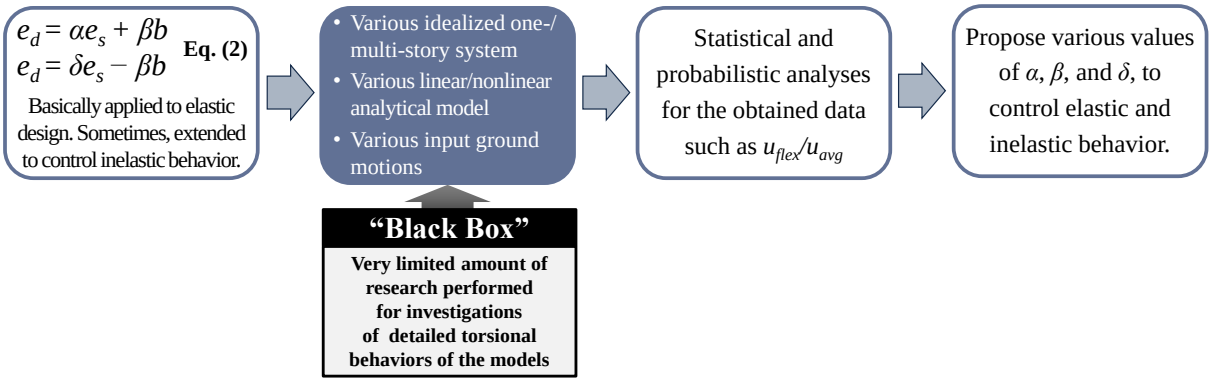

Fig. 3 Typical approach of studies for seismic torsion based on design eccentricity

2. DESIGN OF THE MODEL AND EXPERIMENTAL SETUP

The prototype in Fig. 4 was determined based on the inventory study, and designed by considering the gravity loads only. The reinforcement details are non-seismic, according to construction practice in Korea. The lowest two stories of the 1:5 scale structure model were designed and constructed to strictly satisfy the similitude requirements, while the upper three stories were replaced with concrete blocks of similar volume (Fig. 5). This modified model enabled a reduction in time and cost for construction, without significant loss of similitude in the response.

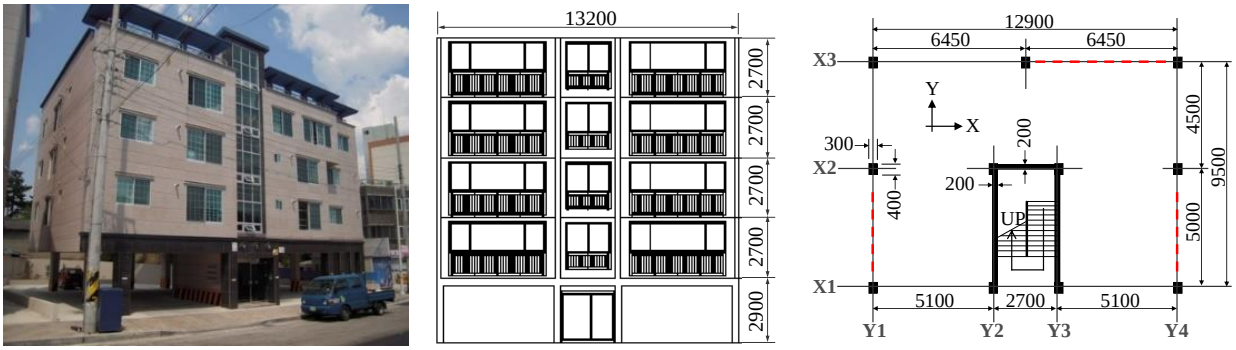

(a) Example of piloti building (b) Elevation (c) Plan of the ground floor

Fig. 4 Prototype structure (unit: mm)

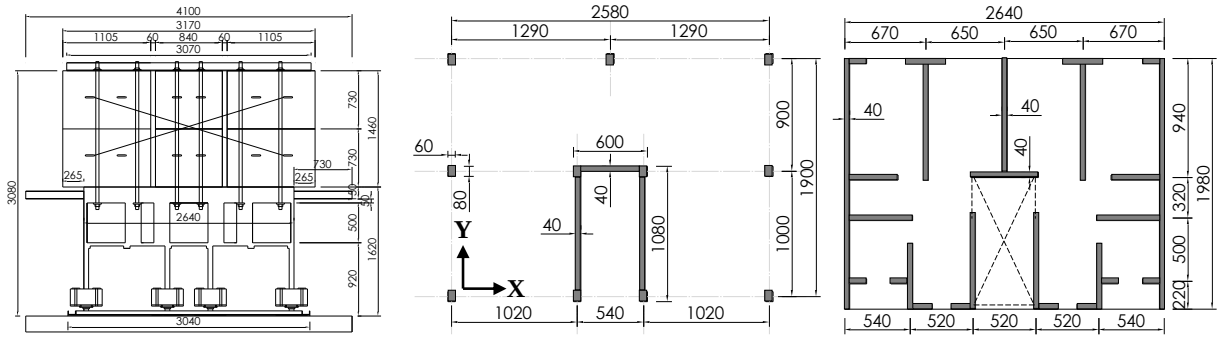

(a) Elevation (b) Plan of ground floor (c) Plan of second floor

Fig. 5 Dimension of 1:5 scale model (unit: mm)

To complement the irregularity of the original model (i.e., soft story, weak story, and torsional eccentricity at the ground story) the prototype was strengthened with buckling-restrained braces (BRB's) and fiber reinforced polymer (FRP) sheets in the peripheral frames. Detailed designs of the BRB's and FRP sheets are provided in Lee et al. (2013). Evaluations of the prototypes regarding the irregularities, in accordance with KBC 2005 (AIK 2005), are provided in Table 1. The degrees of irregularity of the original building were so high at the ground story that even the strengthened building still did not satisfy the requirement for regularity in some cases. The stiffness and strength of the strengthened first story were increased slightly, compared with those of the second story, because the ratio of the wall area to the total floor area at the second story, 10.5%, is much larger than that at the first story 1.93%. However, the strengthened model greatly alleviated the degree of irregularity for the torsion in the Y- direction (Table 1).

Table 1. Assessment of irregularity at the ground story according to KBC2005

Irregularity	Criteria	Original		Strengthened	
		X-dir.	Y-dir.	X-dir.	Y-dir.
Stiffness	If $K_1/K_2 < 0.7$, irregular (NG)	0.159 (NG)	0.160 (NG)	0.218 (NG)	0.213 (NG)
Strength	If $F_1/F_2 < 0.8$, irregular (NG)	0.181 (NG)	0.284 (NG)	0.260 (NG)	0.356 (NG)
Torsion	If $\delta_{max}/\delta_{avg} > 1.2$, irregular (NG)	1.18 (OK)	1.82 (NG)	1.26 (NG)	1.31 (NG)

K_1/K_2: Stiffness of first story / stiffness of second story, F_1/F_2 : Strength of first story / strength of second story, $\delta_{max}/\delta_{avg}$: Maximum / average drift

The design base shear force, *V,* for this strengthened prototype was determined using the following Eqs (3) and (4) with the response modification factor, R = 3, and the occupancy importance factor, I_E =1.2, as defined in KBC 2005:

$$V = C_s \cdot W = 0.176 \cdot 7{,}148 = 1{,}260\ kN \text{ (prototype)} \tag{3}$$

$$C_S = \frac{S_{D1}}{(R/I_E)T_a} = \frac{0.234}{(3.0/1.2)\,0.349} = 0.268\text{, but, not exceeding, } C_S = \frac{S_{DS}}{R/I_E} = \frac{0.439}{3.0/1.2} = 0.176 \tag{4}$$

where C_S is the seismic coefficient; W is the seismic weight of the prototype building (*kN*); S_{DS} and S_{D1} are the spectral accelerations at period 0.2 *s* and 1 *s*, respectively; and T_a is the fundamental period (*sec*). Because the equivalent seismic weight of the 1:5 scale strengthened specimen was 267.4 *kN*, the design base shear of the 1:5 scale model was $V = C_s \cdot W = 0.176 \cdot 267.4 = 47.1\ kN$.

The experimental set-up and instrumentation to measure the displacements, accelerations, and forces for the second series of tests are similar to those of the first series of tests, and are shown in Fig. 6. The target or input accelerogram of the table was based on the recorded 1952 Taft N21E (X direction) and Taft S69E (Y direction) components, and was formulated by compressing the time axis with a scale factor of 1/√5, and by adjusting the peak ground acceleration (PGA), to match the corresponding elastic design spectrum in KBC 2005 (AIK 2005). First, the test was performed with the table excitations in only one direction (X direction), and the consecutive test was conducted in the two orthogonal directions (X and Y directions), for each level of earthquake intensity. The strengthened model was tested not only up to the levels of maximum considered earthquake (MCE) in Korea, but also to the level of the design earthquake in San Francisco, USA. Detailed information on the results of earthquake simulation tests on the original and strengthened model is provided in Lee et al (2011 and 2013). The program of earthquake simulation tests on the strengthened model is summarized in Table 2. The designation and significance of each earthquake simulation test is provided in the table.

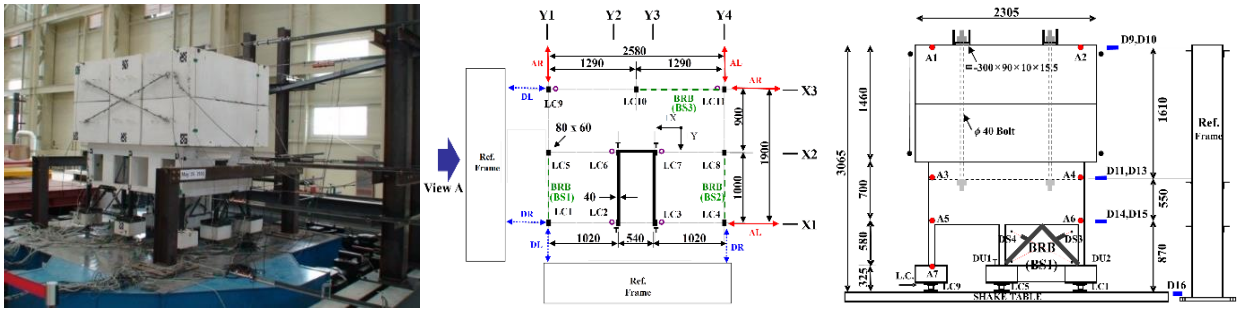

(a) Overview of earthquake simulation test set-up of strengthened model

(b) Plan at the ground story

(c) View A
(D: displacement,
A: acceleration)

Fig. 6 Dimensions and instrumentation of the 1:5 scale structure model (unit: mm)

Table 2. Test program (X-Taft N21E, Y-Taft S69E)

Test designation	Intended PGA(g)		Measured PGA(g)		Return period in Korea (year)
	X-dir.	Y-dir.	X-dir.	Y-dir.	
R0.070X	0.07	-	0.083	-	50 (SLE)
R0.070XY	0.07	0.08	0.072	0.097	
R0.154X	0.154	-	0.132	-	500 Design Earthquake (DE)
R0.154XY	0.154	0.177	0.123	0.186	
R0.187X	0.187	-	0.174	-	
R0.187XY	0.187	0.215	0.147	0.220	
R0.3X	0.3	-	0.261	-	2400 (MCE) DE in San Francisco, USA
R0.3XY	0.3	0.345	0.250	0.374	
R0.4X	0.4	-	0.329	-	
R0.4XY	0.4	0.46	0.442	0.509	

3. SEISMIC INTERACTION BETWEEN SHEAR AND TORSION

The design eccentricity is composed of static and accidental eccentricity (Eq. (2)). In this experimental model, however, the center of mass in the plan was unchanged throughout the tests, and the shake table did not rotate during the earthquake simulation. Thus, in this study, we investigated how the center of resistance (CR) changed in the elastic and inelastic response under uni- and bi-directional excitations, with increasing intensity of the excitations.

Fig. 7 shows the distribution of torsional eccentricity, $e_y=T_x/V_x$, under uni- and bi-directional excitations, which represent the serviceability level of the earthquake (R0.070X, R0.070XY), the design earthquake (R0.187X, R0.187XY), and the maximum considered earthquake (R0.3X, R0.3XY) in Korea. With a very small value of the base shear, the eccentricity will have a highly amplified value. Therefore, the eccentricities in Fig. 10 were computed only for the peak base shear exceeding certain limits, ±15*kN* under R0.070X, ±30*kN* under R0.187X, and ±50*kN* under R0.3X.

In Fig. 7(a), 72% of the eccentricities in the elastic response under uni-directional excitation, R0.070X, were included within a range of ±10% from the average, with 100% and 96% under R0.187X and R0.3X, respectively. The higher the intensity of the excitations with the inelastic response, the more the data points were included within a range of ±5% from the average. That is, the range of the distribution of eccentricities gradually became narrower as the intensity of excitations increased.

In Fig. 7(b), the distributions of data points under the bi-directional excitation were similar to those under the uni-directional excitation. The higher intensity of excitations caused more data points to be included within a range of ±5% from the average.

Fig. 8 shows the seismic interaction between shear and torsion under the serviceability level of the earthquake (SLE, R0.070XY) and the maximum considered earthquake (MCE, R0.3XY) in Korea. The response histories of the X-directional base shear versus torsional moment contributed by the X-directional frames V_x-T_x in the elastic range under R0.070XY (Fig. 8(a)-3) and inelastic range under R0.3XY (Fig. 8(b)-3) appear very chaotic. Despite the chaotic responses in *V*-*T*, the ratio of the torsional moment contributed by the X-directional frames (T_x) to the Y-directional frames (T_y) in the elastic range (Fig. 8(a)-1) is almost constant with the approximate value ratio being 40%:60%.

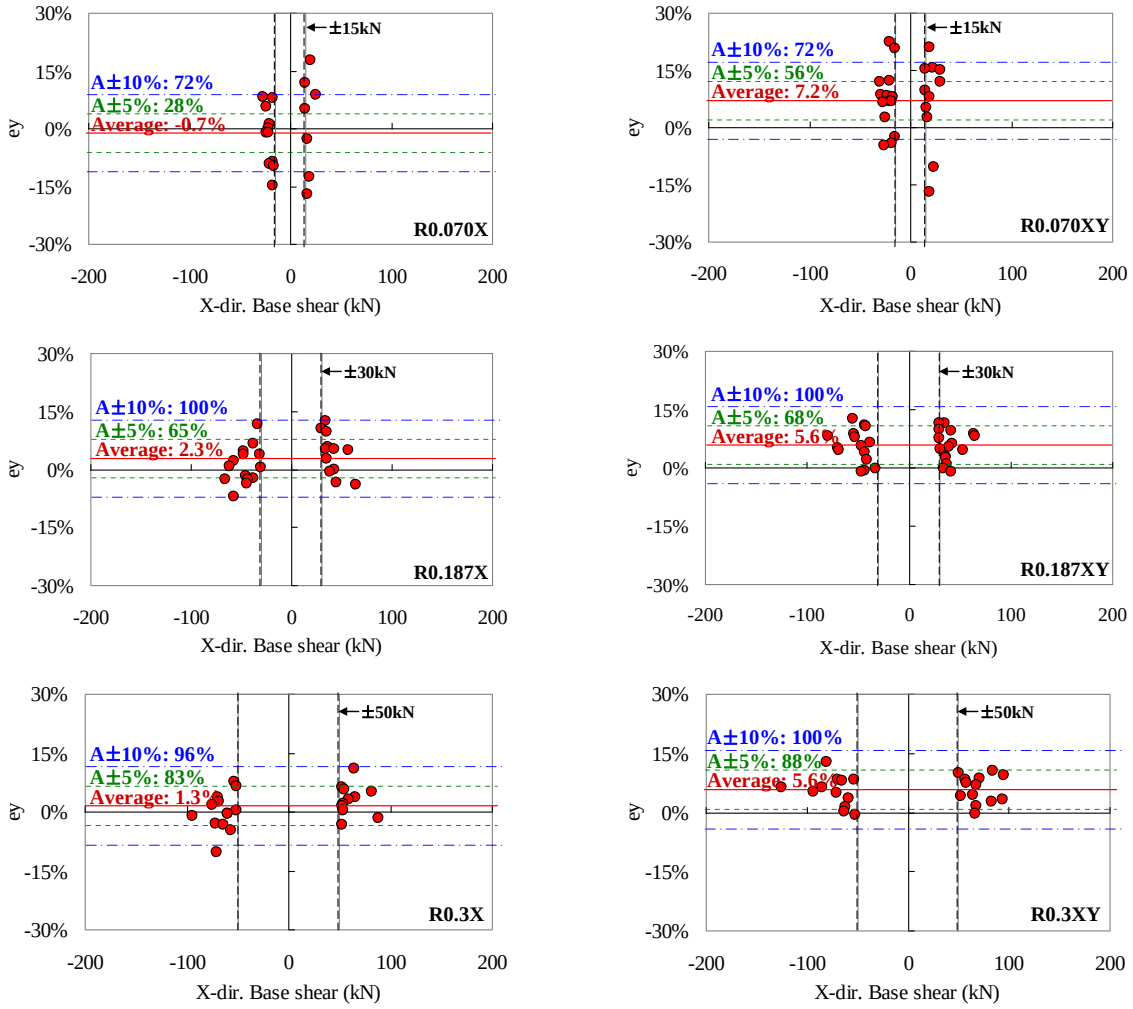

(a) Uni-directional excitations (b) Bi-directional excitations

Fig. 7. Distribution of eccentricities at instants of peak base shear (Lee and Hwang 2015)

However, in the inelastic range (Fig. 8(b)-1), this ratio is no longer constant, but varies. The eccentricity in the X direction, $e_y=T_x/V_x$, appears to be not in a limited range as prescribed in the general codes, but it varied from zero to infinity with the variation of the torsional moment and the base shears for both elastic and inelastic responses. Under MCE in Korea (R0.3XY), the inertial torque varied from –23.1kNm to +27.9kNm and the eccentricity varied from 3.7% to 0.01% with the yielding base shear, 106kN, being almost constant for a short duration from 3.04s to 3.11s (a→(4)→(2)) as shown in Figs. 8(b)-3 and 5. The small eccentricity of 0.01% at time instant (2) did not necessarily translate into a small but significantly large rotation (0.00173rad) leading to the maximum drift (6.2mm) at the edge frame in Fig. 9(b) due to a high level of inertial torque (27.9kNm) and a significantly degraded torsional stiffness caused by yielding of the longitudinal frames (Fig. 8(b)-6). Based on these observations, it becomes clear that the eccentricity in itself cannot represent the real critical torsional behavior as design parameter.

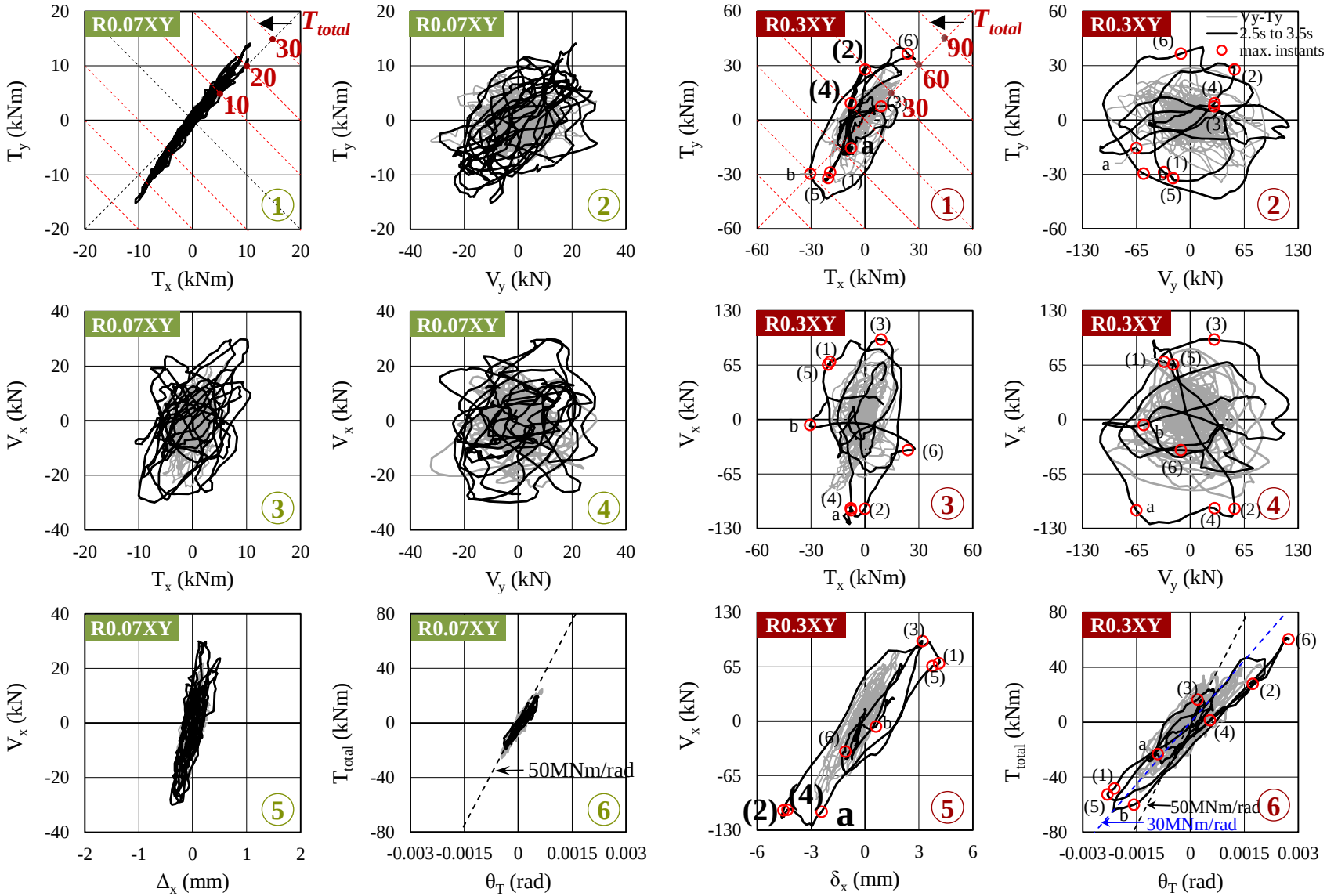

(a) R0.07XY (SLE) (b) R0.3XY (MCE)

Fig. 8 Seismic interaction between shear and torsion

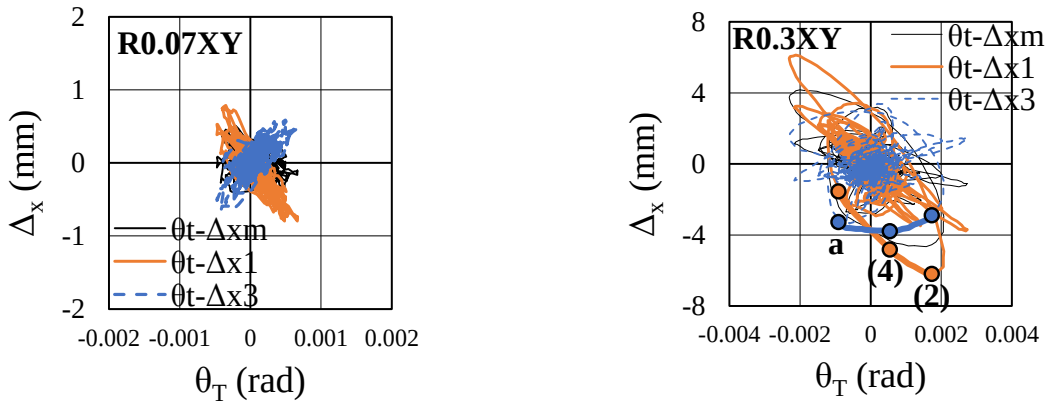

(a) R0.07XY (SLE) (b) R0.3XY (MCE)

Fig. 9 Response histories between the torsional deformation and the first story drift

In Fig. 10, the eccentricity is defined as a distance between the external inertial force and the resisting shear force to represent the torsional responses, i.e. the moment due to two coupled forces, T_y. The value of T_y is not same as that of the total external inertial moment, T_{total} (=T_x+T_y). Therefore, it is clear that, in order for the structure to have the same coupling effect in the Y direction, the external torsion should be applied by the amount of T_{total}. But, the general codes over the world require the application torsion moment T_y only. This is a clear mistake which should be corrected.

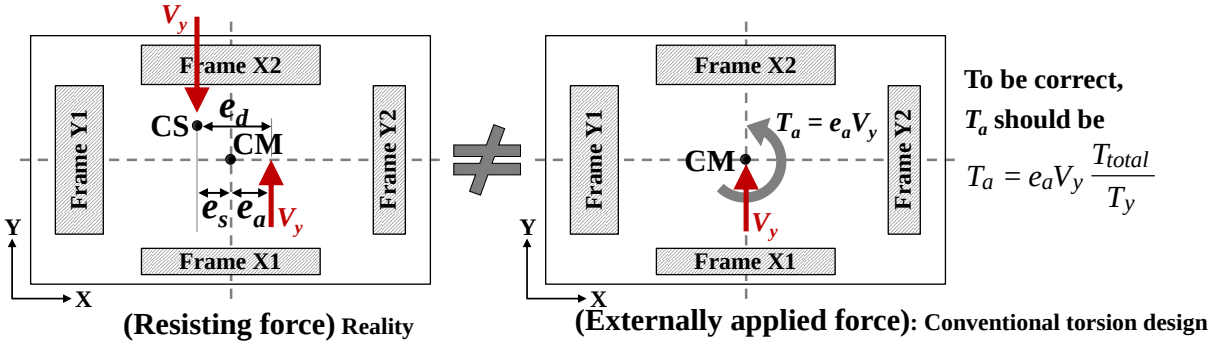

Fig. 10 Confusion in application of design torsional moment

Using the yield strength of each frame in the simplified bilinear force-displacement relation, the yield shear force and yield torsional moment with the yield mechanism are shown by closed envelope line in Fig. 11. It is called the base shear-torque (BST) corresponding yield surface (De la Llera and Chopra 1995b). Fig. 11 also shows the response histories of base shear (V) versus torsional moment (T_{total} & T_y) under the MCE in Korea under R0.3XY. In Fig. 11, the demand (T_{total}) and supply (capacity) for the shear force and the torsional moment are directly compared. The each segment of straight lines in Fig. 11 corresponds to the state of yielding mechanism as depicted beside the lines. In Fig. 11(a), the large X-directional base shears at time instant (2) exceeded the plane EF of the BST surface. In Fig. 11(b), the point “b” in the curves of the Y-directional base shear versus the torsional moment can be found to be near the BST yielding surface. The corresponding states of forces and deformation are given in Fig. 12.

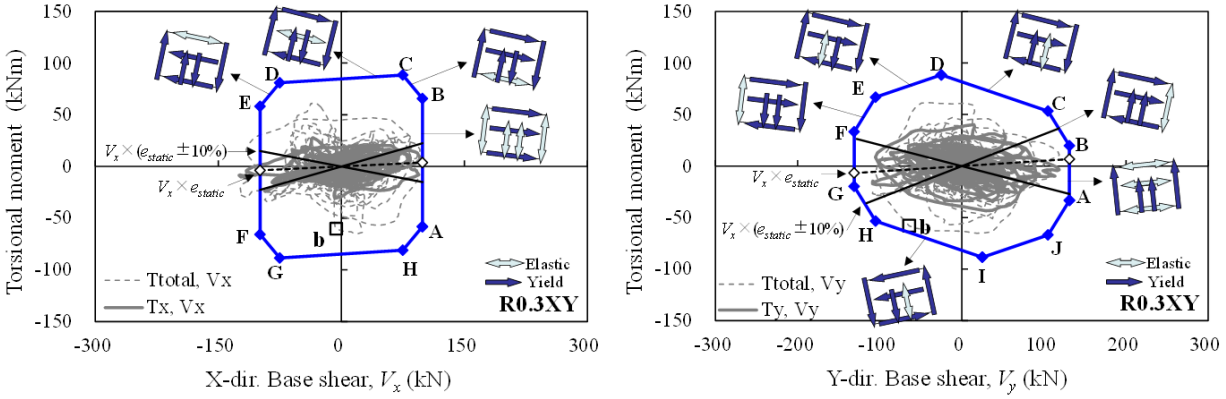

(a) V_x-T (b) V_y-T

Fig. 11 BST yield surface versus V-T response histories under R0.3XY (Lee and Hwang 2015)

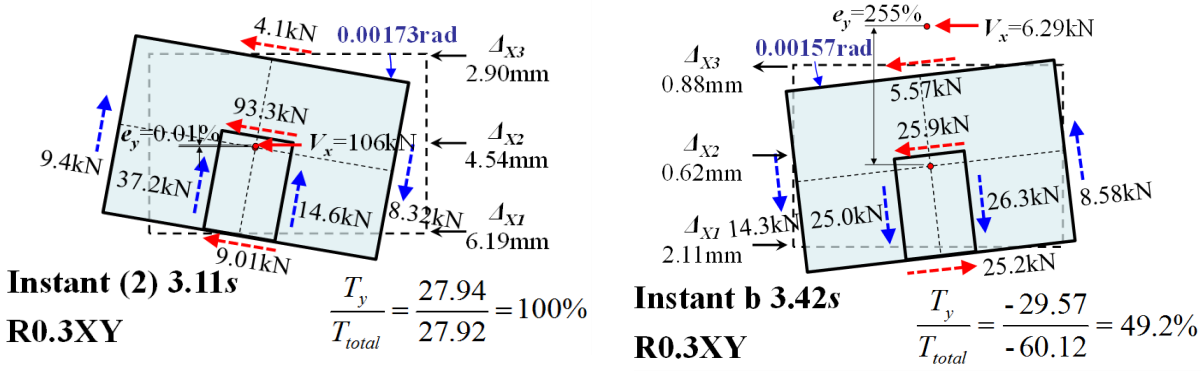

(a) Instant (2) (b) Instant b

Fig. 12 Distribution of frame forces and deformation at time instants (2) and b in Fig. 11 (Lee and Hwang 2015)

4. A New Methodology in Seismic Torsion Design

The actual dynamic coupling existing between lateral and torsional motions in a building with plan asymmetry, named “natural torsion” (Chopra and De la Llera 1996), inevitably leads to non-uniform displacement demands on the lateral resisting planes of the system. Such displacement demands are of key interest in the sizing and detailing of structural elements for earthquake resistance. Fig. 8 shows the relation of torsional moment and base shear, T_x-V_x and T_y-V_y, in the experiment. The eccentricity, which is the slope of the line connecting the zero point and the point (T_x, V_x) varies from zero to infinity at each instant. The experimental relationship contains both natural and accidental torsions. In this experimental model, the accidental torsion includes only the uncertainty on the stiffness of the structures, because the center of mass in the plan was unchanged and the shake table did not rotate throughout the tests. The natural torsion for the experimental model was simulated through the elastic modal time history analysis using SAP2000 (Computers and Structures 2009), using the record of the table acceleration under R0.07X, which is assumed to be the serviceability level for an earthquake in Korea. For the five natural modes of the model which constitute the time

history, the natural periods and modal participating mass ratios are given in Table 3, where the first and second modes are the modes coupled by the translational movement in the X direction and the torsion, while the third is translation in the Y direction. The fourth and fifth are the second translational modes in the X- and Y-directions, respectively. While the participating mass ratio of the X-directional translation, M_{ux}, is 58% with that of the torsion, M_{rz}, being 30% for the first mode, the participating mass ratio of torsion, M_{rz} = 68%, is dominant over that of the X directional translation, 25%, for the second mode.

Table 3. Periods and modal participating mass ratios (*M*) obtained from elastic modal analysis

	Mode 1	Mode 2	Mode 3	Mode 4	Mode 5
Periods (Experiment)*	0.175 sec	0.160 sec	0.142 sec	-	-
Periods (Modal analysis)	0.166 sec	0.157 sec	0.145 sec	0.0546 sec	0.0428 sec
M_{ux}**	58.0 %	25.0 %	0.0 %	17.0 %	0.0 %
M_{uy}**	0.0 %	2.0 %	70.0 %	0.0 %	28.0 %
M_{rz}**	30.0 %	68.0 %	2.0 %	0.0 %	0.0 %

* Periods are obtained from the earthquake simulation test results (time histories of base shear and torsional moment) under R0.07X using Fast Fourier Transforms (FFT) analysis.

** M_{ux} and M_{uy}: the X- and Y directional modal participating mass ratios, respectively.
M_{rz}: the torsional modal participating mass ratio.

Fig. 13 shows that the total analytical relationship generally simulated well the experimental, and that the modal responses in the relationship between the torsional moment and base shear for the (i) first and (ii) second modes, (iii) the combination of the first and the second, and (iv) the comparison of the experimental responses with the total analysis, comprising all the responses of the five modes under R0.070X. In Fig. 13 the torsional moment-base shear responses, T_x-V_x, in modes 1 and 2 reveal the linear relationship. The slope in the T_x-V_x relationship of the first mode, $e_y = T_x/V_x$, is -7.8%, with that of the second mode, $e_y=T_x/V_x$, being 21.5%. The T_x-V_x relationship, combining the first and second modal behaviors, resulted in the elliptical shapes, where the maximum values in base shear and torsional moment in the first and second modes were generally preserved while the eccentricity was no longer constant, but varied from zero to infinity.

This phenomenon is also investigated in the relationship between the torsional deformation and the X-directional interstory drift at the first story, θ - Δ_x, in Fig. 13 (c). The response histories of θ - Δ_x in modes 1 and 2 reveals the linear relationship, and the boundary of the response histories combining the first and second modal behaviors looks like the ellipse. The X-directional interstory drift at the first story, Δ_x, is taken at the geometric center of the plan, and the drifts in the Frames X1 and X3 (Fig. 4(c)) are about twice as larger as Δ_x in Fig. 13(d) and (e).

This elliptical responses reveals the reason for the gap between the values of static eccentricity assumed in the seismic design codes, which generally represent the first translation and torsion coupled mode, and those of the 'real' dynamic eccentricity, that is, the natural eccentricity. It is also noteworthy that the combined modal behaviors, that is, mode 1 + mode 2, approximate roughly the total results of elastic modal analysis, which, in turn, simulate very well the experimental results.

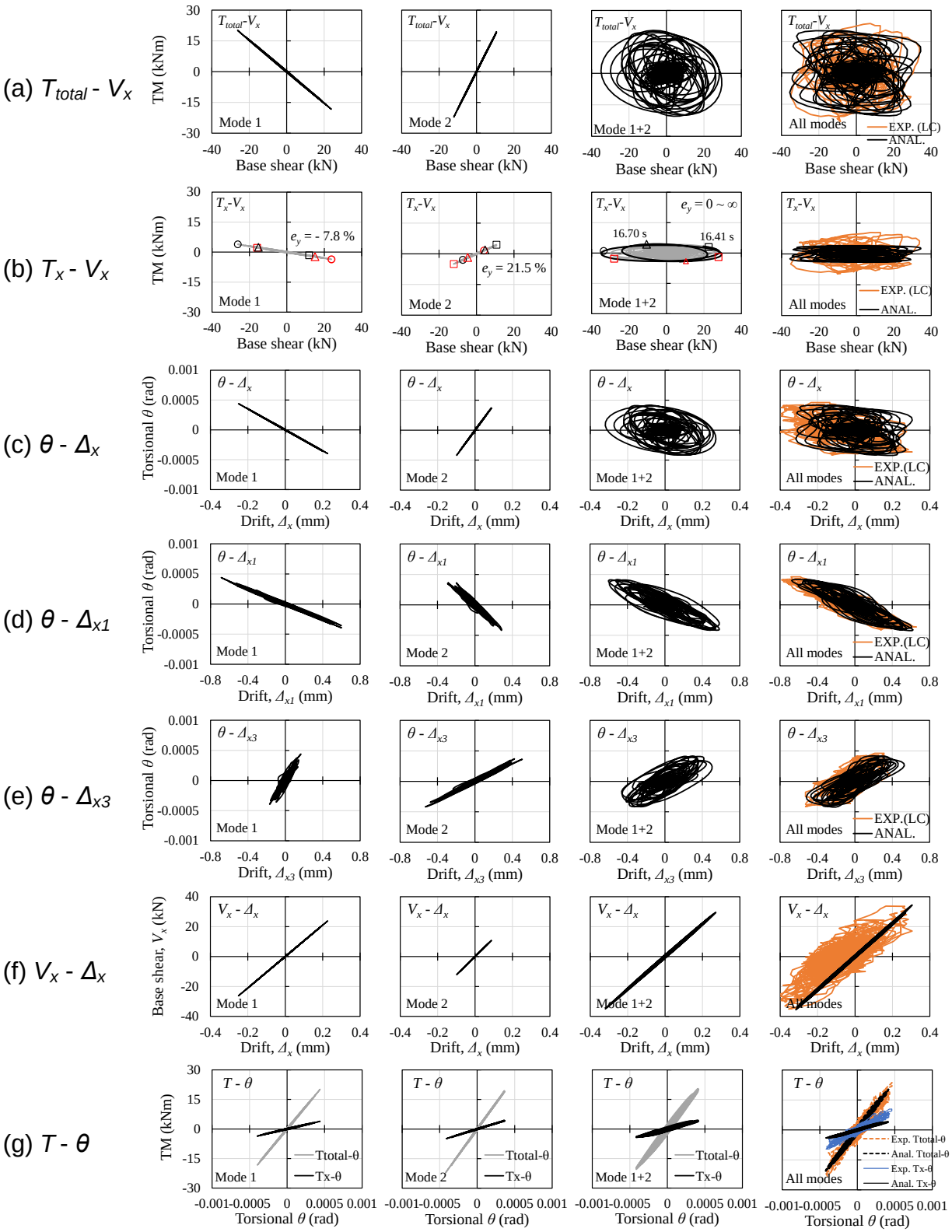

Fig. 13 Results of elastic modal analysis under R0.07X compared with corresponding experiment

Fig. 14 shows an ellipse with the response histories of T_{total}-V_x and θ-Δ_x combining the first and second modal responses and those of modal responses. The ellipse is constructed using the maximum values in the first and second modes in the T_{total}-V_x and θ-Δ_x relationships (Fig. 13). The equation of ellipse can be expressed as the path of a point ($X(t)$, $Y(t)$) in Eq. (5):

$$\begin{aligned} X(t) &= A\ \cos t\ \cos\varphi - B\ \sin t\ \sin\varphi \\ Y(t) &= A\ \cos t\ \sin\varphi + B\ \sin t\ \cos\varphi \end{aligned} \tag{5}$$

where, t is the parametric angle, $0 \le \theta \le 2\pi$; A is radius in the major axis; B is the radius in the minor axis; and φ: the angle between the X-axis and the major axis of the ellipse. The parameters A, B, and φ in Eq. (5) are given in Table 4. We can find that the constructed ellipse cover reasonably the actual response histories.

Table 4. Parameters in equation of ellipse (Eq. (5)) for shear-torsion relationships

Relationship of Ellipse		$X(t)$: Shear		$Y(t)$: Torsion		A	B	ϕ
		1st mode	*2nd mode*	*1st mode*	*2nd mode*			
Serviceability level for EQ. in Korea (R0.07X) (Fig. 13)	Force*	$V_{x,max1}$	$V_{x,max2}$	$T_{total,max1}$	$T_{total,max2}$	1.41	1.19	-0.785
		26.3	12.1	20.1	22.1			
	Deformation*	$\Delta_{x,max1}$	$\Delta_{x,max2}$	θ_{max1}	θ_{max2}	1.41	1.03	-0.785
		0.25	0.098	0.000439	0.000419			
Design values (Fig. 14)	Force*	V_{D1}	V_{D2}	T_{D1}	T_{D2}	1.41	1.11	-0.785
		68.1	29.3	52.3	53.3			

* Unit of force, V and T: kN and kNm, respectively; Unit of deformation, Δ and θ: mm and rad, respectively.

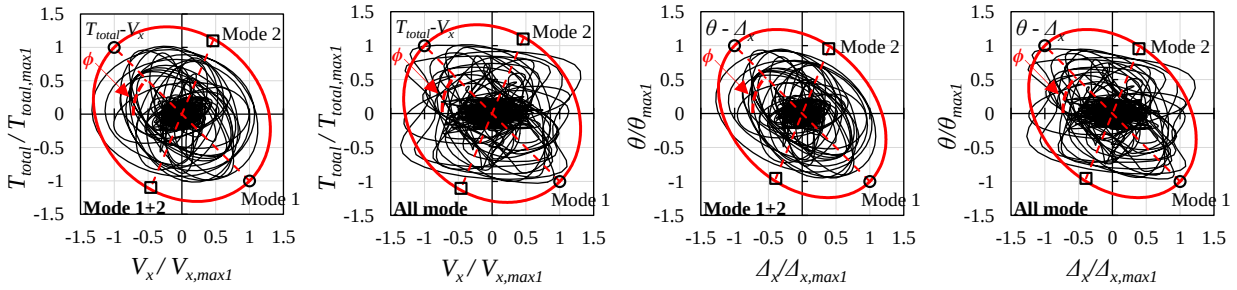

(a) Force relationship (b) Deformation relationship

Fig. 14 Shear-torsional force and deformation relationship under R0.07X

In Fig. 15(a), the demand is an ellipse with two adjacent torsion-dominant modal spectral values (Table 4) using the design response spectrum and the periods of structures obtained from the elastic modal analysis (Table 3):

$$V_{D1} = C_s M_{ux1} W = 68.1\text{kN};\ \text{and}\ V_{D2} = C_s M_{ux2} W = 29.3\text{kN} \tag{6}$$

$$T_{D1} = s_1 V_{D1} = 52.3\text{kNm};\ \text{and}\ T_{D2} = s_2 V_{D1} = 53.3\text{kNm} \tag{7}$$

where, the V_{D1} and V_{D2} are the design base shear in the first and second modes, respectively; the C_s is obtained by the design response spectrum (Fig. 15(b)); the M_{ux1} and M_{ux2} are modal participating mass ratios (X-dir.) given in Table 3; the W is the seismic weight; the T_{D1} and T_{D2} are the design torsional moment in the first and second modes, respectively; and the s_1 and s_2 are the slope of the T_{total}-V_x relationship in the first and second modes, respectively.

Comparing the ellipse with the BST yield surface, as given in Fig. 11(a), the elliptical demand is within the BST yield surface (capacity). This approach provides a simple and transparent conceptual design tool through comparison with the torsion capacity diagram given as BST or SST yield surfaces without having to perform dynamic time history analyses.

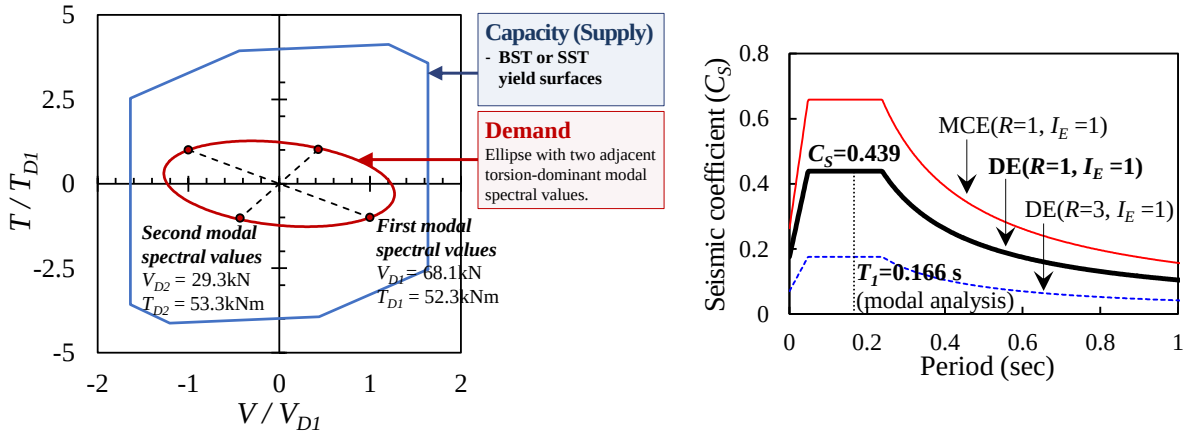

(a) Design diagram (b) Design response spectrum

Fig. 15 Design diagram using shear force-torque relationship with design spectrum

The torsion design approach in Fig. 15(a) is developed based on the elastic behavior. However, the main concern in the torsion design is the control of the deformation and damage in the inelastic range rather than those in the elastic range.

Based on the experimental results, the conceptual design diagram is extended to ultimate SST surface and inelastic elliptical demand as shown in Fig. 16. In the inelastic range, the main axis of the elliptical demand becomes closer to the axis of shear force, and tends from stiffness eccentricity to strength eccentricity. It is expected that, in most cases of *V*-*T* demand in inelastic range, the maximum point of the shear force exceeds the bound of the yield SST surface, but within the ultimate SST surface. In such cases, the inelastic behavior (maximum drift or ductility demands) should be checked by comparison with the allowable limits given in the design codes.

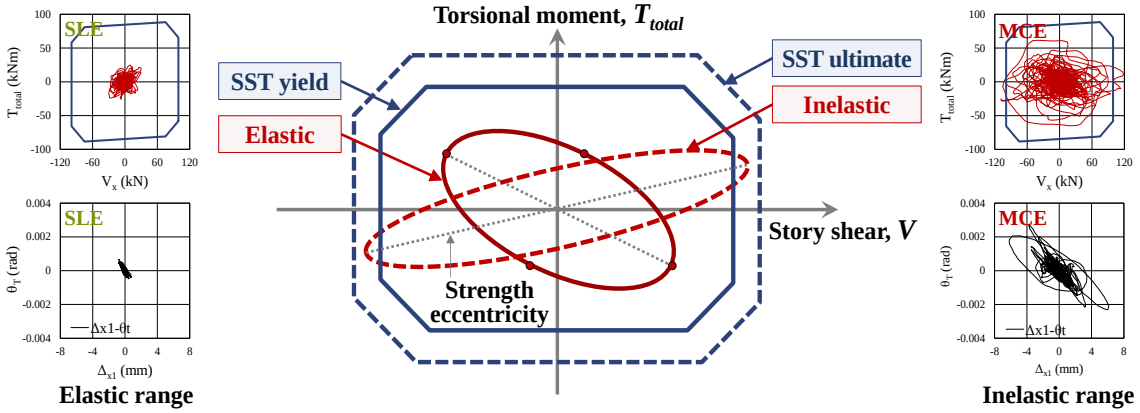

Fig. 16 Conceptual design approach comparing yield and ultimate SST (story shear–torque) surfaces to elastic and inelastic elliptical demands

To estimate the story drift (δ) and torsional deformation (θ) in the inelastic range, De la Llera and Chopra (1994) suggested the force-deformation relation as follows:

The inelastic behavior is assumed to be governed by elasto perfectly plastic behavior and, hence, it can be described by the well-known constitutive relations:

$$v = v^e + v^p \tag{6}$$

$$F = Kv^e \tag{7}$$

$$\dot{v}^p = \dot{\lambda}\eta \tag{8}$$

where, v, v^e, v^p represent the total, elastic, and plastic deformations at a given instant; $\dot{v}^p$ is the plastic deformation rate; $\dot{\lambda}$ is a plastic parameter determined by the loading-unloading criterion; and η is the plastic flow direction .

The plastic parameter λ is computed from the criterion for loading and unloading from the SST surface, which is assumed to satisfy the Kuhn-Tucker conditions, i.e.

$$\dot{\lambda}\Phi(F) = 0, \quad \dot{\lambda} \geq 0, \quad \Phi(F) \leq 0 \tag{9}$$

where, $\Phi(F)$ is the functional form of the SST surface. The three conditions in Eq. (9) must be satisfied simultaneously during any loading process. If $\Phi(F)<0$, the first equation implies that $\dot{\lambda} = 0$ and, hence, the behavior is elastic. Contrarily, if $\dot{\lambda} > 0$, then $\Phi(F)=0$ and the system is on the SST ultimate surface. During plastic deformation, the system cannot go beyond the SST ultimate surface, which defines the so-called plastic consistency condition:

$$\dot{\Phi}(F) = \frac{\partial \Phi^T}{\partial F}\dot{F} = 0 \tag{10}$$

where, the vector $\partial\Phi/\partial F$ represents the gradient of the SST surface. As shown in Fig. 17(c), the step goes into the plastic range, and the elasto-plastic matrix for branch m (K_m^{ep}) on SST ultimate surface is defined in Eq. (11):

$$K_m^{ep} = K - \frac{(\partial\Phi/\partial F)_m (\partial\Phi/\partial F)_m^T K}{(\partial\Phi/\partial F)_m^T K (\partial\Phi/\partial F)_m} \tag{11}$$

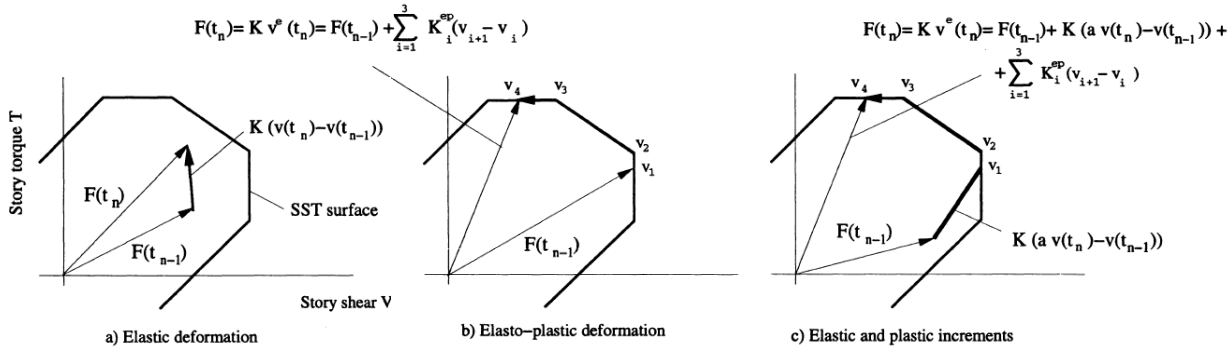

Fig. 17 Integration of constitutive elasto-plastic relationship (De la Llera and Chopra 1994)

5. CONCLUSIONS

This study proposed a new methodology in the seismic design and control of torsionally unbalanced building structures. The followings are main features of this paper:

(1) Earthquake simulation tests on a 1:5 scale five-story RC building model with the irregularity of a soft/weak story and torsion at the ground story revealed that the eccentricity was not within the range specified by the code design eccentricity, but varied from zero to infinity and that even very small eccentricity can lead to the significantly large drift at the edge frame under the severe earthquake. These findings mean that the design eccentricity specified by the general codes can represent neither the real or "natural" eccentricity, nor the critical parameter to control the damage or drift due to torsion.
(2) The inertial or external torsion was resisted by both T_x (contributed by the longitudinal frames) and T_y (contributed by transverse frames). The ratio between T_x:T_y remained constant in the elastic response. Because the torsion due to eccentricity in one direction covers only the torsion contributed by that corresponding directional frames, the equivalent external torsion (T_a) due to the accidental eccentricity (e_a) should be $T_a=e_aV_X \times(T_{total}/T_X)$ instead of $T_a=e_aV_X$ as specified in the general seismic codes.
(3) To overcome the inappropriateness of the eccentricity as design parameter for torsion, a new methodology in the torsion design of torsionally unbalanced building structure is proposed by defining the design torsional moment in a direct relationship with the shear force given as an ellipse with the maximum points in its principal axes located by the two adjacent torsion-dominant modal spectral values. This paper demonstrates an example.
(4) The proposed torsion design approach is developed based on the elastic behavior. However, the main concern in the torsion design is the control of the deformation and damage in the inelastic range rather than those in the elastic range. Based on the experimental results, the conceptual design diagram is extended to ultimate SST surface (capacity) and inelastic elliptical demand. To estimate the story drift and torsional deformation in the inelastic range, an inelastic analysis procedure proposed by De la Llera and Chopra (1994) is introduced in this paper.

ACKNOWLEDGMENTS

The research presented herein was supported by the National Research Foundation of Korea, through the contracts NRF-2007-0054740 and NRF-2009-0078771. The authors are grateful for these supports.

REFERENCES

Anagnostopoulos, S.A., Kyrkos, M.T., and Stathopoulos, K.G. (2013), “Earthquake induced torsion in buildings: critical review and state of the art”. *Plenary keynote lecture in 2013 World Congress on Advances in structural engineering and mechanics (2013 ASEM Congress)*.

Architectural Institute of Korea (AIK) (2005). Korean Building Code. *KBC 2005*. Seoul, Korea. (in Korean)

Chandler, A. M., Duan, X. N. and Rutenberg, A. (1996), "Seismic torsional response: Assumptions, controversies and research progress", *Europ. Earthq. Eng.* **10**(1): 37-51.

Chopra A.K. and De la Llera J.C. (1996). “Accidental and Natural Torsion in Earthquake Response and Design of Buildings”. *Proceedings of 11th world conference on earthquake engineering*, Paper No. 2006, Acapulco, Mexico.

Computers and Structures Inc. (2009). SAP 2000 [Software]. Computers and Structures, Inc.: Berkeley, CA.

De la Llera, J.C., and Chopra, A.K. (1994), *Accidental and Natural Torsion in Earthquake Response and Design of Buildings*. Report No. UCB/EERC-94/07.

De la Llera, J.C., and Chopra, A.K. (1995a), “Estimation of accidental torsion effects for seismic design of buildings”. *Journal of Structural engineering*, **121**(1), 102-114.

De la Llera, J.C., and Chopra, A.K. (1995b), “Understanding the inelastic seismic behavior of asymmetric-plan buildings”. *Earthquake Engineering and Structural Dynamics*, **24**:549–572.

Lee, H.S., Jung, D.W., Lee, K.B., Kim, H.C., and Lee, K. (2011). “Shake-table responses of a low-rise RC building model having irregularities at first story”, *Structural Engineering & Mechanics*, **40**(4), 517-539.

Lee, H.S., Lee, K.B., Hwang, K.R., and Cho, C.S. (2013). “Shake-table Responses of an RC Low-rise Building Model Strengthened with Buckling Restrained Braces at Ground Story”. *Earthquakes & Structures*, **5**(6), 703-731.

Lee, H.S. and Hwang, K.R. (2015), “Torsion design implications from shake-table responses of an RC low-rise building model having irregularities at the ground story”. *Earthquake Engng Struct. Dyn.,* **44**, 907–927.

Rutenberg, A. (1992), "Nonlinear response of asymmetric building structures and seismic codes: A State of the Art", *Europ. Earthq. Eng*. VI(2): 3-19